CHEMICAL ENGINEERING TRANSACTIONS
VOL. 62, 2017
A publication of AIDIC
The Italian Association of Chemical Engineering
Online at www.aidic.it/cet
Guest Editors: Fei Song, Haibo Wang, Fang He

ISBN 978-88-95608- 60-0; **ISSN** 2283-9216
DOI: 10.3303/CET1762039

Research on Using Mechanical and Chemical Methods to Synthesize Lithium Battery Electrode Materials

Huomei Zhu, Jingjie Tu, Yubin Zhang, Huanpei Lv

Ningbo Dahongying University, Ningbo 315175, China
zhuhuomei@126.com

In order to study the influence of mechanical and chemical treatment on the performance of SiO_2 negative electrode materials, this paper prepares SiO_2 negative electrode materials by mechanical ball milling. The nanopowder of different ball milling periods is analyzed by X-ray diffraction (XRD), field emission scanning electron microscope, and constant current charge and discharge test and other methods. The XRD analysis shows that the crystallization of SiO_2 increases with time which changes completely to amorphous state after 80h. According to the SEM observation, the SiO_2 particle size decreases and becomes more uniform with the increasing ball milling time. According to the electrochemical test, the reversible lithium storage capacity of SiO_2 increases with the increasing ball milling time, of which the sample after 80h of ball milling has the best comprehensive electrochemical performance with the 1st lithium storage capacity under current density of 100mAg-1 up to 1440.7mAhg-1 and the 1st coulomb efficiency of 53.8%. After 100 cycles, the reversible capacity increases from 188.4mAhg-1 of the pristine SiO_2 to 571.4mAhg-1.

1. Introduction

With the increasing shortage of traditional energy and the increasingly serious environmental problems today, "substitute electricity for oil" is one of the effective ways to solve the above problems and achieve "low-carbon lifestyle". With high energy density, long cycle life, low self-discharge and other advantages, lithium-ion batteries are of great importance in solving the energy crisis and environmental pollution, becoming the focus of power materials research and development all over the world (Anders et al., 2017). Negative electrode materials are the core component of lithium-ion batteries and one of the key factors that directly determine the electrochemical performance of lithium-ion batteries (Dong et al. , 2016). In recent years, silicon receives extensive concern due to its high specific capacity as a cathode material, but its cycle performance is poor for it may break and fall off due to volume effect in use (Espinoza-González et al., 2016). Whereas SiO_2 has the advantages of all silicon-based materials without the volume effect, it is gradually becoming a highly potential negative electrode material.

Mechanical and chemical synthesis method is to form superfine powder by interaction between different elements or compounds through high energy ball milling (Esrin, 1984), which is a new method mainly used in the preparation of immiscible alloy (Ezrin, 1984), amorphous materials and nanocrystalline materials (Kim et al., 2014). Its characterized by introducing plenty of strains and defects in the mechanization process to make it transformed to metastable structures far from the equilibrium state (Ghahrizjani et al., 2016), which is different from regular solid reaction (Gulyakova et al., 2017). In recent years, mechanical chemistry theories and technology are developing rapidly presenting shows a tempting prospect in the theoretical research and new material development with mechanical and chemical methods widely used in the preparation of high-performance lithium ion structural materials (Rao et al., 2016).

2. Experimental method

2.1 Raw materials and equipment

The materials for the experiment were commercial SiO_2 (purity: analytically pure), argon (purity: 99.99%) and anhydrous alcohol (purity: 99.99%), etc. The ball miller is of planetary type with stainless steel ball mill tank

Please cite this article as: Huomei Zhu, Jingjie Tu, Yubin Zhang, Huanpei Lv, 2017, Research on using mechanical and chemical methods to synthesize lithium battery electrode materials, Chemical Engineering Transactions, 62, 229-234 DOI:10.3303/CET1762039

and milling balls of GGr15 (Laurita et al, 2017). Milling balls of 6mm, 10mm and 15mm were mixed in the ratio of 20:10:1(Lee, 2017). Other equipment involved in the experiment were vacuum drying oven, vacuum glove box, electronic scale, etc.

2.2 Experimental procedure

First, dry 2g SiO_2 powder in the vacuum oven at 80 °C for 4 h, and then put it into an 80ml ball mill tank with a milling ball around 50:1 to the material in mass (Lenoir, 2017). Next, transfer the ball mill tank to a Braun glove box with Ar atmosphere of high purity for sealing (Li and Wan, 2017). To control the ball mill atmosphere (Lin, et al., 2017), the partial pressures of H2O and $_2$ were both lower than 1ppm in the glove oven (Liu et al., 2017). In the ball milling, alternate forward and reverse operation was adopted with a fixed speed of 500r/min. Operation of 30min was followed by a pause 10min in each ball milling cycle, after which another cycle was initiated for the reverse operation to ensure the ball milling temperature is close to the room temperature (Mai and Wang, 2014). The total ball milling duration ranged from 10h to 80h. After that, take out the samples of different ball milling durations for later test (Meshginqalam and Alaei, 2017).

Mix the ball mill powder, the conductive agent (acetylene black) and the binder (sodium carboxymethyl cellulose) in the mass ratio of 60:30:10 (Ng et al., 2017) and then put them into a magnetic stirrer for intense stirring for 1h before applying it on copper foil for vacuum drying at 120°C for 12 hours (Rao et al., 2017). After the electrode was dried, soak it in the electrolyte for 12 hours. As with the button battery assembly, the order from the bottom to the top was positive electrode shell -cathode -diaphragm - lithium tablet- collector - supporting chip - negative electrode shell (Suganya et al., 2017). Let the battery stand for one day before further tests.

2.3 Sample testing method

Cu-Kα radiation source with a wave length of 1.5406Å was adopted in the X-ray powder diffraction experiment (XRD) to continuously scan to collect data (Sultana et al., 2017), with a 2θ range of 10-80°, tube current of 40mA, tube voltage of 40kV, scan rate of 20°/min and scanning step length of 0.033°. Morphology of SiO_2 materials prepared in different conditions were observed and analyzed in the field emission scanning electron microscope experiment (SEM) (Suzuki et al., 2017). In preparing samples, mix appropriate powder materials with alcohol solution in a certain proportion for ultrasonic dispersion, then suck up the suspension and drop it on the aluminum test-bed for drying before further tests (Yao et al., 2014). The constant current charge and discharge test took the lithium tablet as the electrode with a charging and discharging range of 0.01-3.0V and time interval of 5min (Yao et al., 2015). The current density of the constant current test was 100mAg-1, and that of the multiplier performance test 100-2000mAg-1(Zheng and Moskal, 2012)). The scanning voltage range of the cyclic voltammetry test was 0.0-3.0V with a scan rate of 0.1 mV/s and test temperature 30°C (Zheng et al., 2017).

3. Experiment result

3.1 Phase analysis

Figure 1 shows the XRD patterns of pristine SiO_2 and its milled products of different periods. It can be seen from the figure that pristine SiO_2 has the smallest semi-height width and the strongest peak strength. After the 20h of ball milling, the XRD diffraction peak intensities weakens obviously with the semi-height width starting to widen and this continues with time. When the ball mill time is extended to 40h, the diffraction peak intensity of the sample stops changing significantly, since it has changed to an amorphous state.

3.2 Morphology analysis

Figure 2 shows the SEM images of pristine SiO_2 and samples milled for 12-72h. As shown in Figure 2 (a), the pristine SiO_2 material are particles with irregular appearance with particle sizes above 5μm as well as some small particles with particle sizes of 200-500nm. After 20h of ball milling, large particles of the material began to split to smaller pieces, resulting in a small proportion of large particles. Among them, larger particle size ranges from 2-4μm and smaller particle size from 200-500nm, as shown in Figure 2(b). When the ball milling period is increased to 80h, the overall dispersion of particle size begins to become uniform and stable, with most of the particle sizes within the range of 200-300nm, as shown in Figure 2(c). It can be quantitatively determined from the size change of the particles that with the decreasing material particle size and particle concentration of larger particles, the specific surface area of the material is constantly increasing accordingly. Therefore, the SiO_2 material of submicron structure with uniform appearance and most particle sizes below 300nm is prepared by mechanical ball milling.

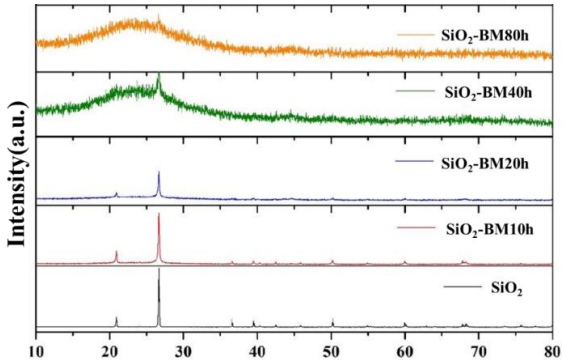

Figure 1: XRD patterns of pristine SiO_2 and its milled products of different periods

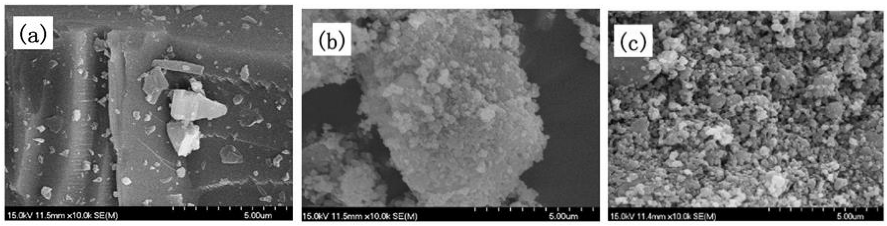

(a) SiO_2 (b) SiO_2-BM20h (c) SiO_2-BM80h

Figure 2: SEM images of pristine SiO_2 and samples milled for different periods of time

3.3 Electrochemical performance analysis

Voltage profiles of 1st cycle for pristine SiO_2 and samples after different periods of milling is shown in Figure 4.3. It can be seen from the figure that 1st discharge capacity of the pristine crystalline SiO_2 is less than 300mahg-1, but the material presents a higher initial discharge capacity after being milled for some time. As the ball milling time increases from 10 to 40 h, the 1st reversible capacity of the materiaI increases gradually, which is 387.7mAhg-1 at 10h, 532.1mAhg-1 at 20h and 834.4 mAhg-1 at 40h, but after 80h it begins to decrease to 783.2 mAhg-1. As the ball milling time increases, the 1st Coulomb increases from the 40.5% at 10h and reaches 53.8 at 80h. See Table 1 for detailed initial charge and discharge capacity of pristine SiO_2 and materials after different periods of milling and initial Coulomb efficiency.

Table 1: Electrochemical properties of pristine SiO_2 and samples after different periods of milling

Time (h)	First Li / Li removal capacity ($mAhg^{-1}$)	First Coulomb efficiency (%)	Capacity of 50 cycles ($mAhg^{-1}$)	Capacity of 100 cycles ($mAhg^{-1}$)
0	295.6/163.3	55.2	194.3	188.4
10	952.3/387.7	40.5	432.8	380.6
20	1220.5/532.1	53.9	530.1	410.3
40	1742.5/834.4	47.2	599.4	508.1
80	1440.7/783.2	53.8	625.3	571.4

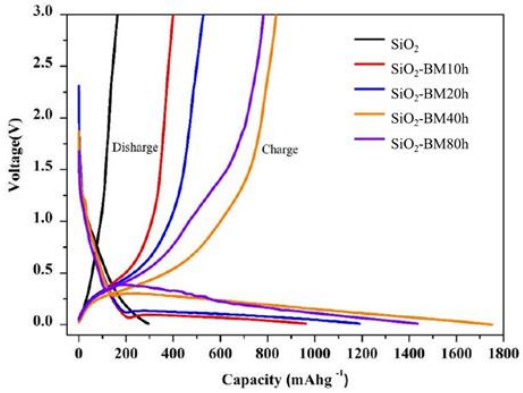

Figure 3: Voltage profiles of 1st cycle for pristine SiO_2 and samples after different periods of milling

Figure 4 shows the cycle performance of pristine SiO_2 and SiO_2 after different periods of ball milling. It can be seen from the figure, the material capacity gradually tends to be kept at a higher level as the ball milling time increases, especially the sample after 80h of ball milling, which is significantly improved compared with the pristine sample. Although the pristine SiO_2 material and SiO_2 material after 10h's ball milling excels in capacity retention, the lithium storage capacity remains in a lower level due to failing in or incomplete lithium intercalation in the material itself. The discharge capacity of the pristine SiO_2 sample after 50 cycles is 194.3mAhg-1 and 188.4mAhg-1 after 100 cycles. The discharge capacity of the SiO_2 sample with 10h of ball milling after 50 cycles is 432.8mAhg-1 and 380.6mAhg-1 after 100 cycles, which are still significantly lower than those of samples with longer ball milling. The SiO_2 materials after 40h and 80h of ball milling both suffer greater capacity loss within the first 30 cycles before maintaining a higher level. The capacities are 599.4mAhg-1and 625.3mAhg-1 respectively after 50 cycles and 508.1mAhg-1 and 571.4mAhg-1 after 100 cycles.

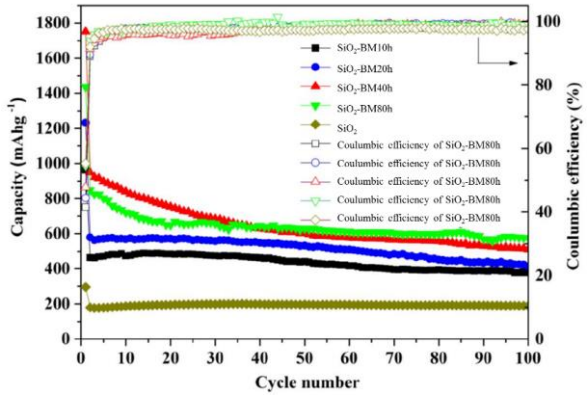

Figure 4: Cycling performance of pristine SiO_2 and samples after different periods of milling

4. Analysis and discussion

It can be seen from the 1st discharge curve of Figure 3 that there is a gentle slop at around 0.7V during the 1st discharge process, which is resulted from the electrolyte decomposition and the SEI film formation. There are also tilting platforms at 0.1- 0.4V for SiO_2 electrode materials with different ball milling periods. This part of capacity is resulted from SiO_2 lithium-intercalation reaction, which is probably caused by the formation of Li2O, Si and LixSi alloy.

For the cycle performance difference, the pristine SiO_2 material has larger particles with uneven distribution, resulting in fewer lithium ion channels while the SiO_2 material after 10h of ball milling still has a greater proportion of particles unevenly distributed than refined particles. Since there is crystalline phase scattering inside both samples, the stress at various directions are uniform, which buffers the volume expansion during the charge and discharge of the materials to a certain extent. Therefore, the cycle stability of both samples at early stage is better than that of the samples with longer milling periods. SiO_2 materials after 40h and 80h of ball milling both present high cycle stability even after 100 cycles. But due to their complete amorphization, the

buffer phase within the materials decreases, resulting in rapid capacity loss in the early stage. In contrast, the sample after 40h of ball milling has remaining Crystalline phase, so the capacity loss in the first 15 cycles is slower.

5. Conclusion

With commercial SiO_2 as the raw material, this paper prepares SiO_2 powders of different particle sizes by ball milling. The influence of milling periods on particle size, morphology and distribution of the materials are systematically studied, revealing the mechanism of how they affect the electrochemical lithium storage performance of SiO_2 materials. As ball milling time increases, the particle size of the pristine SiO_2 material decreases and the specific surface area gradually increases. The material was basically in the crystalline state within 10h of ball milling, which was low, though higher than that of the pristine SiO_2 material. After the 20h and 40h of ball milling, most materials began to transform into amorphous state. The particle sizes of the materials were further decreased with the electrochemical properties improved significantly. After 80h of ball milling, the materials were completely transformed into amorphous state with uniform particle size distributing basically within 300nm. The capacity of SiO_2 increased significant with the increasing ball milling time from less than 200mAhg-1 of the pristine material after 100 cycles to 571.4mAhg-1 after 80h of ball milling. The rate capability was also significantly improved. The performance improvement is mainly due to the ball milling which reduces the particle size of the materials, narrows the distance of lithium ion dispersion and increases the paths, relieving the volume effect during the charge and discharge processes to some extent.

Acknowledgements

This paper is supported the follow projects: (1) Provincial Science and Technology (No.2014C31163); (2) Provincial Department of Education Research (Item No.Y201432654).

Reference

Anders S., Schmelz M., Franke D., Stolz R., Meyer H.G., 2017, Chemical --Mechanically Planarized Cross-Type Josephson Junctions in Nb-Al-AlOx-Nb Technology, IEEE Transactions on Applied Superconductivity, 27, 1-4, DOI: 10.1109/TASC.2017.2685498

Dong X.R., Sun X.Y., Chu D.K., Yin K., Luo Z., Zhou C., Wang C., Hu Y.W., Duan J.A., 2016, Microcavity Mach --Zehnder Interferometer Sensors for Refractive Index Sensing, IEEE Photonics Technology Letters, 28, 2285-2288, DOI: 10.1109/LPT.2016.2591983

Espinoza-González C., Ávila-Orta C., Martínez-Colunga G., Lionetto F., Maffezzoli A., 2016, A Measure of CNTs Dispersion in Polymers with Branched Molecular Architectures by UDMA, IEEE Transactions on Nanotechnology, 15, 731-737, DOI: 10.1109/TNANO.2016.2530697

Esrin M., Gartner J., 1984, Test Method for Evaluation of the Resistance of Fiberglass Rods to Combined Mechanical and Chemical Stress, IEEE Transactions on Power Apparatus and Systems, PAS-103, 2741-2745, DOI: 10.1109/TPAS.1984.318249

Ezrin M., Gartner J., 1984, Test Method for Evaluation of the Resistance of Fiberglass Rods to Combined Mechanical and Chemical Stress, IEEE Power Engineering Review, PER-4, 60-61, DOI: 10.1109/MPER.1984.5525831

Ghahrizjani R.T., Sadeghi H., Mazaheri A., 2016, A Novel Method for onLine Monitoring Engine Oil Quality Based on Tapered Optical Fiber Sensor, IEEE Sensors Journal, 16, 3551-3555, DOI: 10.1109/JSEN.2016.2523805

Gulyakova A.A., Gorokhovatsky Y.A., Frübing P., Gerhard R., 2017, Relaxation processes determining the electret stability of high-impact polystyrene/titanium-dioxide composite films, IEEE Transactions on Dielectrics and Electrical Insulation, 24, 2541-2548, DOI: 10.1109/TDEI.2017.006587

Rao C., Singh A.P., Saravanan M., Varaprasad B., 2016, Plasma-Generated Etchback to Improve the Via-Reliability in High-Tg Substrates Used in Multilayer PWBs for Space Electronic Packaging, Packaging and Manufacturing Technology IEEE Transactions on Components, 6, 926-932, DOI: 10.1109/TCPMT.2016.2548943

Laurita R., Miserocchi A., Ghetti M., Gherardi M., Stancampiano A., Purpura V., Melandri D., Minghetti P., Bondioli E., Colombo V., 2017, Cold Atmospheric Plasma Treatment of Infected Skin Tissue: Evaluation of Sterility, Viability, and Integrity, IEEE Transactions on Radiation and Plasma Medical Sciences, 1, 275-279, DOI: 10.1109/TRPMS.2017.2679010

Lee S.W., Chen K.N., 2017, Development of Bumpless Stacking With Bottom --Up TSV Fabrication, IEEE Transactions on Electron Devices, 64, 1660-1665, DOI: 10.1109/TED.2017.2657324

Lenoir G., Aubin V., 2017, Mechanical Characterization and Modeling of a Powder-In-Tube MgB2 Strand, IEEE Transactions on Applied Superconductivity, 27, 1-5, DOI: 10.1109/TASC.2016.2629481

Li Y., Wan W., 2017, Exploring Polymer Nanofiber Mechanics: A review of the methods for determining their properties, IEEE Nanotechnology Magazine, 11, 16-28, DOI: 10.1109/MNANO.2017.2708819

Lin A.S., Parashar P., Yang C.C., Huang W.M., Huang Y.W., Jian D.R., Kao M.H., Chen S.W., Shen C.H., 2017, High Mechanical Strength Thin HIT Solar Cells with Graphene Back Contact, IEEE Photonics Journal, 9, 1-9, DOI: 10.1109/JPHOT.2017.2750487

Liu J.P., Beyca O.F., Rao P.K., Kong Z.J., Bukkapatnam S.T.S., 2017, Dirichlet Process Gaussian Mixture Models for Real-Time Monitoring and Their Application to Chemical Mechanical Planarization, IEEE Transactions on Automation Science and Engineering, 14, 208-221, DOI: 10.1109/TASE.2016.2599436

Mai T., Wang Y., 2014, Adaptive Force/Motion Control System Based on Recurrent Fuzzy Wavelet CMAC Neural Networks for Condenser Cleaning Crawler-Type Mobile Manipulator Robot, IEEE Transactions on Control Systems Technology, 22, 1973-1982, DOI: 10.1109/TCST.2013.2297405

Meshginqalam B., Alaei S., 2017, Investigation of Molecular Adsorption Effect on the Electrical Properties of CNT-Based Sensors, IEEE Sensors Journal, 17, 3776-3781, DOI: 10.1109/JSEN.2017.2697682

Ng J., Chen Q., Xie Y.H., Wang A., Wu T., 2017, Comparative study between the fracture stress of poly- and single-crystalline graphene using a novel nanoelectromechanical system structure, IET Micro Nano Letters, 12, 907-912, DOI: 10.1049/mnl.2017.0422

Rao C., Wang T., Peng Y., Cheng J., Liu Y., Lim S.K., Lu X., 2017, Residual Stress and Pop-Out Simulation for TSVs and Contacts in Via-Middle Process, IEEE Transactions on Semiconductor Manufacturing, 30, 143-154, DOI: 10.1109/TSM.2017.2688498

Suganya S., Kumar P.S., Saravanan A., 2017, Construction of active bio-nanocomposite by inseminated metal nanoparticles onto activated carbon: probing to antimicrobial activity, IET Nanobiotechnology, 11, 746-753, DOI: 10.1049/iet-nbt.2016.0234

Sultana S., Ahmad N., Faisal S.M., Owais M., Sabir S., 2017, Synthesis, characterisation and potential applications of polyaniline/chitosan-Ag-nano-biocomposite, IET Nanobiotechnology, 11, 835-842, DOI: 10.1049/iet-nbt.2016.0215

Suzuki Y., Hichri H., Wei F., Sundaram V., Tummala R., 2017, Embedded Trench Redistribution Layers at 2 -- 5 μ m Width and Space by Excimer Laser Ablation and Surface Planer Processes for 20 -- 40 μ m I/O Pitch Interposers, Packaging and Manufacturing Technology IEEE Transactions on Components, 7, 838-845, DOI: 10.1109/TCPMT.2017.2676023

Yao Y., Tey J.N., Li Z., Wei J., Bennett K., McNamara A., Joshi Y., Tan R.L.S., Ling S.N.M., Wong C.P., 2014, High-Quality Vertically Aligned Carbon Nanotubes for Applications as Thermal Interface Materials, Packaging and Manufacturing Technology IEEE Transactions on Components, 4, 232-239, DOI: 10.1109/TCPMT.2013.2296370

Yao Y., Lu G.Q., Boroyevich D., Ngo K.D.T., 2015, Survey of High-Temperature Polymeric Encapsulants for Power Electronics Packaging, Packaging and Manufacturing Technology IEEE Transactions on Components, 5, 168-181, DOI: 10.1109/TCPMT.2014.2337300

Zheng G., Moskal L.M., 2012, Leaf Orientation Retrieval from Terrestrial Laser Scanning (TLS) Data, IEEE Transactions on Geoscience and Remote Sensing, 50, 3970-3979, DOI: 10.1109/TGRS.2012.2188533

Zheng Y., Ling D., Wang Y.W., Jang S.S., Tao B., 2017, Model Quality Evaluation in Semiconductor Manufacturing Process with EWMA Run-to-Run Control, IEEE Transactions on Semiconductor Manufacturing, 30, 8-16, DOI: 10.1109/TSM.2016.2630705